2D NMR Observation of Strain-Induced β-Form in Poly[(*R*)-3-hydroxybutyrate]

Yusuke Nishiyama,*,† Toshihisa Tanaka,‡ Toshio Yamazaki,† and Tadahisa Iwata*,‡

Genomic Sciences Center, RIKEN Institute, Tsurumi-ku, Yokohama, Kanagawa 230-0045, Japan, and Polymer Chemistry Laboratory, RIKEN Institute, 2-1 Hirosawa, Wako-shi, Saitama 351-0198, Japan

Received February 8, 2006; Revised Manuscript Received April 3, 2006

ABSTRACT: The first NMR observation of the planar zigzag conformation (β-form) in a poly[(*R*)-3-hydroxybutyrate] uniaxially oriented film with high tensile strength is reported. A ^{13}C two-dimensional (2D) off-magic-angle spinning NMR method which directly correlates the peak positions with the molecular orientation in uniaxially oriented samples was used. The 2D NMR spectra provide the ^{13}C carbonyl signal of β-form separately from that of the 2/1 helix conformation (α-form). The orientations of the carbonyl carbons for α-form and β-form were determind and compared to the previously proposed molecular models.

Introduction

Poly[(*R*)-3-hydroxybutyrate] (P(3HB)) (Figure 1) is accumulated by a wide variety of microorganisms for intracellular carbon and energy storage[1] and has been extensively studied as a biodegradable and biocompatible thermotropic polymer.[2−4] However, it is well-known that the mechanical properties of P(3HB) homopolymer films and fibers deteriorate markedly by a process of secondary crystallization,[5,6] and therefore attempts to improve the mechanical properties have been perfomed.[7−10]

Recently, Iwata and co-workers succeeded in processing uniaxial P(3HB) homopolymer films[11−13] and fibers[14,15] with a high tensile strength by new drawing processes including cold drawing and two-step drawing. In these samples, the molecules are highly aligned relative to each other, and the crystallinity is high. Since the molecular mobility tends to decrease in such a polymer, the secondary crystallization process is avoided and the mechanical properties are improved.

The X-ray fiber diagrams of P(3HB) highly oriented films and fibers indicated the existence of two types of molecular conformations of P(3HB): the 2/1 helix conformation (α-form)[16] and the planar zigzag conformation (β-form),[12,13,16,17] as shown in Figure 2. P(3HB) generally crystallizes in a $P2_12_12_1$ orthorhombic space group with unit cell parameters $a = 0.576$ nm, $b = 1.320$ nm, and c(fiber axis) $= 0.596$ nm, and the molecular chains are left-handed 2/1 helix conformation (α-form). β-form is introduced by the orientation of free chains in the amorphous regions between α-form lamellar crystals and is responsible for the good mechanical properties of the P(3HB) films and fibers.[17,18] β-form was first observed by a wide-angle X-ray diffraction measurement (WAXD) of a further drawn, uniaxially stretched P(3HB) homopolymer film[16] and a cold-drawn film of poly[(*R*)-3-hydroxybutyrate-*co*-21%-(*R*)-3-hydroxyvalerate] (PHB/V).[17] X-ray fiber diagrams of these samples revealed a layer line streak and equatorial reflections, which were not expected from the α-form structure. These new reflections were interpreted as those of β-form. A β-form model was proposed on the basis of an empirical energy calculation with a fiber repeat length of 0.460 nm, which was obtained from the layer line streak.[17] However, no experimental observations of the molecular conformation of β-form have been reported. Furthermore, no other methods besideds WAXD have detected β-form in the P(3HB) films and fibers; ^{13}C magic angle spinning (MAS) NMR, differential scanning calorimetry, and other methods were unsuccessful.

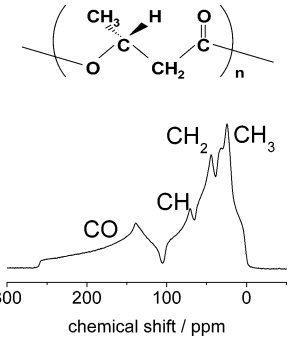

Figure 1. Chemical structure and 1D ^{13}C NMR spectrum (under static conditions) of poly[(*R*)-3-hydroxybutyrate].

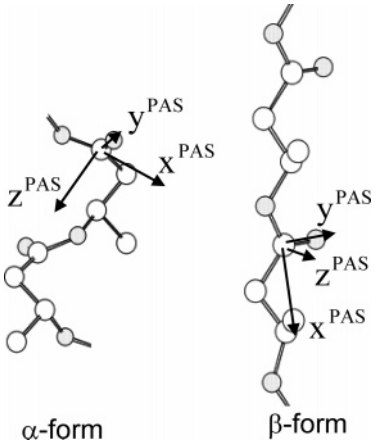

Figure 2. Molecular conformation and PAS orientation for CSA interactions of the carbonyl carbons in α-form and β-form of P(3HB).

In this paper, we present the first solid-state NMR observation of β-form in uniaxially drawn P(3HB) films. The method relies on orientation-dependent NMR frequencies due to chemical shift anisotropy (CSA). The principal values and orientation of the CSA tensor are crucial for the analysis. It is well-known that

† Genomic Sciences Center.
‡ Polymer Chemistry Laboratory.
* To whom correspondence should be addressed. E-mail: nishi@gsc.riken.jp (Y.N.), tiwata@riken.jp (T.I.).

10.1021/ma060291h CCC: $33.50
Published on Web 05/17/2006

the principal axis system (PAS) of CSA for a carbonyl carbon is nearly fixed to the ⟩C═O plane and is unlikely to be affected by the molecular conformation.[19−22] A well-defined PAS orientation is useful for a structural analysis. Moreover, the large CSA value (ca. ∼150 ppm) of the carbonyl carbon ensured high angular resolution. We obtained one-dimensional (1D) ^{13}C NMR spectra by rotating uniaxially oriented P(3HB) films along their drawn axis at an off-magic angle. The peak position in this spectrum is designated as $\bar{\sigma}$. $\bar{\sigma}$ varies with changing tensor orientation of ^{13}C CSA. Since the orientation of the carbonyl CSA tensor in *β*-form is different from that in α-form (see Figure 2), the carbonyl carbon signal of *β*-form will appear at a different position from that of α-form in the 1D NMR spectra. Thus, we can separately observe the signals from α-form and those from *β*-form. We also observed two-dimensional (2D) ^{13}C NMR spectra by a method for uniaxially oriented samples.[23] This method achieves further separation of the signals and also provides full information on the orientation of the CSA tensor. We observed 2D NMR spectra by recoupling ^{13}C CSA under sample rotation. The 2D spectra thus obtained correlate a CSA parameter ($\bar{\sigma}$) and another CSA parameter (σ_2). The CSA tensor orientation is directly obtained from the $\sigma_2/\bar{\sigma}$ 2D spectra, with the knowledge of the CSA principal values, which can be obtained by observing unoriented α-form samples. Thus, we can obtain the orientations of the carbonyl carbon and uniquely determine the molecular conformation.

NMR Background

We assume that the solid sample in a rotor rotates at an angular velocity ω_r in the magnetic field. The resonance frequency $\omega(t)$, due to the CSA interaction, can be written as[23]

$$\omega(t) = \omega_0[\bar{\sigma}(\alpha_{PR}, \beta_{PR}) + \sigma_1(\alpha_{PR}, \beta_{PR}) \sin(\omega_r t + \delta_1 + \gamma_{PR}) + \sigma_2(\alpha_{PR}, \beta_{PR}) \sin 2(\omega_r t + \delta_2 + \gamma_{PR})] \quad (1)$$

where ω_0 is the Larmor frequency. The Euler angles of $\Omega_{PR} = (\alpha_{PR}, \beta_{PR}, \gamma_{PR})$ define the rotation from PAS, which is fixed to the molecule, to the rotor fixed frame with the z^{rot} axis parallel to the rotor axis. The γ_{PR} angle describes the orientation of PAS around the rotor axis. δ_1 and δ_2 are phase factors from ref 23. σ_1, σ_2, and $\bar{\sigma}$ are CSA parameters independent of γ_{PR} but dependent on (α_{PR}, β_{PR}) as well as β_{RL}, which describes the angle between the rotor axis and the magnetic field:[23]

$$\bar{\sigma} = \sigma^{iso} + P_2(\cos\beta_{RL})\left[P_2(\cos\beta_{PR})(\sigma_{zz}^{PAS} - \sigma^{iso}) + \frac{1}{2}\sin^2\beta_{PR}\cos 2\alpha_{PR}(\sigma_{xx}^{PAS} - \sigma_{yy}^{PAS})\right] \quad (2)$$

$$\sigma_1 = \sin\beta_{RL}\cos\beta_{RL}\sin\beta_{PR}[\{\cos\beta_{PR}[-3(\sigma_{zz}^{PAS} - \sigma^{iso}) + \cos 2\alpha_{PR}(\sigma_{xx}^{PAS} - \sigma_{yy}^{PAS})]\}^2 + [\sin 2\alpha_{PR}(\sigma_{xx}^{PAS} - \sigma_{yy}^{PAS})]^2]^{1/2} \quad (3)$$

and

$$\sigma_2 = \frac{1}{2}\sin^2\beta_{RL}\left\{\left[\frac{3}{2}\sin^2\beta_{PR}(\sigma_{zz}^{PAS} - \sigma^{iso}) + \frac{1}{2}(1 + \cos^2\beta_{PR})\cos 2\alpha_{PR}(\sigma_{xx}^{PAS} - \sigma_{yy}^{PAS})\right]^2 + [\cos\beta_{PR}\sin 2\alpha_{PR}(\sigma_{xx}^{PAS} - \sigma_{yy}^{PAS})]^2\right\}^{1/2} \quad (4)$$

where σ_{jj}^{PAS} ($j = x, y, z$) are the principal values of the CSA tensor and $\sigma_{iso} = (\sigma_{xx}^{PAS} + \sigma_{yy}^{PAS} + \sigma_{zz}^{PAS})/3$ is the isotropic chemical shift. In a 1D experiment, the $\bar{\sigma}$ term gives the centerband at $\bar{\sigma}$, and the σ_1 and σ_2 terms vanish except for the spinning sidebands. In the case that β_{RL} is equal to θ_m, which is the magic angle (MAS), $\bar{\sigma}$ converges on σ_{iso} under MAS and contains no information on (α_{PR}, β_{PR}, γ_{PR}), as shown in eq 2; the resonance frequency is free from orientation distribution, thus resulting in sharp peaks even for disordered samples.

We assume a uniaxially oriented sample in which the molecules are rotationally distributed around the symmetry axis, and the sample is packed into the rotor such that the symmetry axis coincides with the rotor axis. In the uniaxially oriented sample, the PAS orientation is described by fixed (α_{PR}, β_{PR}) angles, and the γ_{PR} angles are uniformly distributed; the (α_{PR}, β_{PR}) angles specify the PAS orientation in the rotor-fixed frame, and γ_{PR} has no information on the molecular orientation. If the γ_{PR} dependence of the resonance frequency is removed, then the analysis of the uniaxially oriented samples is greatly simplified. The sample rotation averages out the γ_{PR}-dependent terms, and the centerband appears at $\bar{\sigma}(\alpha_{PR},\beta_{PR})$. In the case of $\beta_{RL} \neq \theta_m$ (off-magic angle spinning (OMAS)), $\bar{\sigma}$ depends on (α_{PR}, β_{PR}). While a 1D OMAS NMR spectrum of a sample with a distributed orientation yields a broad resonance due to the (α_{PR}, β_{PR}) distribution, a 1D OMAS NMR spectrum of a uniaxially oriented sample provides a sharp peak, reflecting a unique (α_{PR}, β_{PR}) value. Signals for different conformations could appear at different positions. However, the 1D OMAS NMR experiment, i.e., $\bar{\sigma}(\alpha_{PR}, \beta_{PR})$, is not sufficient to completely describe the two parameters of (α_{PR}, β_{PR}). Another CSA parameter that is independent of $\bar{\sigma}(\alpha_{PR}, \beta_{PR})$ is needed.[24]

Here, we introduce a 2D NMR method for determining the CSA tensor orientation.[23] We focused on $\sigma_2(\alpha_{PR}, \beta_{PR})/\bar{\sigma}(\alpha_{PR}, \beta_{PR})$ 2D NMR methods. The σ_2 term is independent of $\bar{\sigma}$. The 1D $\bar{\sigma}$ spectrum is two-dimensionally expanded along the new axis of σ_2, and the $\sigma_2/\bar{\sigma}$ spectrum yields a two-dimensionally distributed signal. The σ_2 dimension can be achieved by a *γ*-encoding CSA recoupling sequence which recouples the σ_2 term and decouples the $\bar{\sigma}$ and σ_1 terms.[25] Note that γ_{PR} dependence is removed for both the σ_2 and $\bar{\sigma}$ dimensions. Thus, the 2D $\sigma_2/\bar{\sigma}$ spectrum of a uniaxially oriented sample shows a sharp peak. Now, we can determine (α_{PR}, β_{PR}) from the peak position.[23] The broadening of the peak is attributed to the distribution of the orientation $P(\alpha_{PR}, \beta_{PR})$. We can determine $P(\alpha_{PR}, \beta_{PR})$ by comparing experimental spectra with simulated spectra.

Spectral Simulation

The Euler angles Ω_{PR}, representing the PAS orientation in the rotor-fixed frame, are needed in order to calculate the spectra. Here, we introduce the crystal frame with the z^{cry} axis parallel to the chain axis, which is equivalent to the crystal *c*-axis. The molecular model can be conveniently described in the crystal frame. Moreover, the crystal frame greatly facilitates the management of the distribution of the crystal orientations as mentioned below. We used the Euler angles $\Omega_{PC}(\alpha_{PC}, \beta_{PC}, \gamma_{PC})$, which transform PAS to the crystal frame, and $\Omega_{CR}(\alpha_{CR}, \beta_{CR}, \gamma_{CR})$, which transform the crystal frame to the rotor-fixed frame. We set $\gamma_{PC} = 0$ without a loss of generality. The rotation defined by Ω_{PR} can be determined by two successive rotations:

$$R(\Omega_{PR}) = R(\Omega_{CR})R(\Omega_{PC}) \quad (5)$$

Ω_{PC} represents the PAS orientation in the crystal frame. The PAS orientation is closely related to the molecular conformation. For the carbonyl carbon, it is known that σ_{22} (y^{PAS}) tends to lie along the C═O bond axis, that σ_{33} (z^{PAS}) tends to lie along the axis perpendicular to the O═C−C plane, and that σ_{11} (x^{PAS})

tends to lie in the O═C−C plane.[19−22] Thus, we can determine Ω_{PC} from the orientation of the O═C−C moiety in the crystal frame.

Ω_{CR} describes the crystal orientation in the rotor-fixed frame. The chain axis aligns along the *c*-axis (z^{cry}) in uniaxially drawn P(3HB) samples.[16] The chain axis is parallel to the z^{rot} axis, i.e., the rotor axis, in uniaxially oriented and perfectly aligned samples, and thus the z^{cry} axis aligns along the z^{rot} axis:

$$P(\alpha_{CR}, \cos\beta_{CR}, \gamma_{CR}) = \delta(\beta_{CR}) \tag{6}$$

where α_{CR} and γ_{CR} are uniformly distributed, and $\delta(\beta_{CR})$ is the delta function. The orientation is not perfectly uniform in the most uniaxially drawn samples; the z^{cry} axis is distributed around the drawn axis. Moreover, the misalignment of uniaxially drawn fibers and films in the sample tube results in discrepancies between the drawn axis and the z^{rot} axis. We introduce the z^{cry} axis distribution in the rotor-fixed frame to account for these effects:[26]

$$P(\alpha_{CR}, \cos\beta_{CR}, \gamma_{CR}) = \exp\left(-\frac{\sin^2\beta_{CR}}{2\sigma_{\beta_{CR}}^2}\right) \tag{7}$$

We used the distribution symmetric with respect to $\beta_{CR} = \pi/2$, since the NMR method cannot discriminate signals for β_{CR} from those for $\pi - \beta_{CR}$. When the molecules are uniformly distributed (isotropic powder), the distribution can be obtained by inserting $\sigma_{\beta_{CR}} \rightarrow \infty$ into eq 7:

$$P(\alpha_{CR}, \cos\beta_{CR}, \gamma_{CR}) = 1 \tag{8}$$

The simulated 2D spectra can be calculated by

$$S(\sigma_2', \bar{\sigma}') = \int\int\int d\alpha_{CR}\, d\cos\beta_{CR}\, d\gamma_{CR}\, P(\alpha_{CR}, \cos\beta_{CR}, \gamma_{CR})\delta(\sigma_2' - \sigma_2(\alpha_{PR},\beta_{PR}))\delta(\bar{\sigma}' - \bar{\sigma}(\alpha_{PR},\beta_{PR})) \tag{9}$$

where $\sigma_2(\alpha_{PR}, \beta_{PR})$ and $\bar{\sigma}(\alpha_{PR}, \beta_{PR})$ are obtained by using (α_{CR}, β_{CR}) and (α_{PC}, β_{PC}) with eq 5. We used a 5000 REPULSION angle set for (α_{CR}, β_{CR})[27] in the calculation. A Lorentzian line broadening of 200 Hz was applied to the simulated spectra. We calculated 2D spectra for various (α_{PC}, β_{PC}) and determined the (α_{PC}, β_{PC}) angles by comparing the 2D calculated spectra and the 2D experimental spectra. Note that there are degeneracies α_{PC}, $\alpha_{PC} + \pi$, $2\pi - \alpha_{PC}$, and $\pi - \alpha_{PC}$ and β_{PC} and $\pi - \beta_{PC}$ under the crystal distribution of eq 7. We represent the orientation uniquely by limiting the ranges of α_{PC} and β_{PC} to $0 \le \alpha_{PC} < \pi/2$ and $0 \le \beta_{PC} < \pi/2$.

Figure 3 schematically represents the 1D and 2D NMR spectra of uniaxially oriented and unoriented samples. The crystals in the uniaxially drawn samples align around the drawn axis as in eq 7. This restricts the Ω_{PR} orientation via eq 5. The signals in the 1D and 2D spectra thus obtained appear at a restricted region, as schematically represented in Figure 3a; a sharp peak appears in the 1D and 2D spectra. Since the peak position is related to the molecular conformation (Ω_{PC}) as described in eqs 1 and 5, the spectrum of a sample with a different molecular conformation shows a peak at a different position (Figure 3b). While the 1D $\bar{\sigma}$ spectra do not provide sufficient information on the molecular orientation, the additional σ_2 axis in the 2D $\sigma_2/\bar{\sigma}$ spectra enables us to determine the molecular conformation; we can obtain (α_{PC}, β_{PC}) angles by simulating the 2D spectra. As the uniaxial orientation deteriorates ($\sigma_{\beta_{CR}}$ becomes large), the NMR line shape gets broadened. When the crystal orientation (Ω_{CR}) is uniformly distributed as in eq 8 ($\sigma_{\beta_{CR}} \rightarrow \infty$), a broad isotropic powder pattern instead of a sharp peak appears in the 1D and 2D spectra, as schematically shown in Figure 3c. The distribution conceals information on the molecular conformation, i.e., the molecular orientation in the crystal frame (Ω_{PC}); the NMR spectra do not contain information on Ω_{PC} since the molecular orientation in the rotor-fixed frame, which determines the NMR resonance frequency, is uniformly distributed regardless of Ω_{PC}.

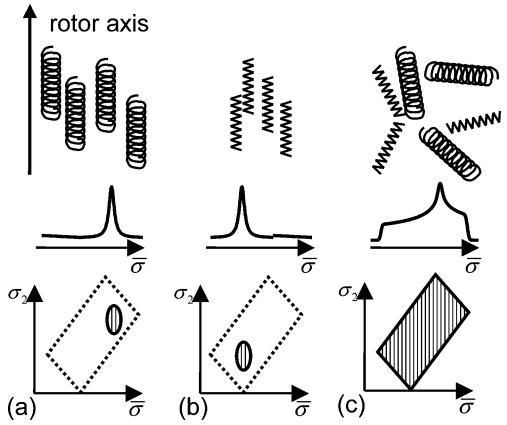

Figure 3. Schematic representation of the crystal orientation and the 1D/2D NMR spectra. The crystals are uniaxially oriented in (a) and (b) with different molecular conformations and are uniformly distributed in (c).

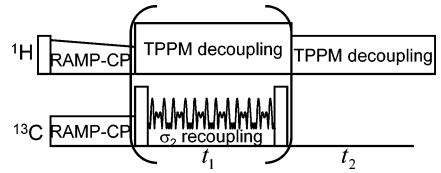

Figure 4. Rf sequences for 1D and 2D OMAS NMR observations of uniaxially oriented samples. 1D NMR spectra were observed immediately after RAMP-CP. 2D NMR spectra were obtained by inserting the $MR6_5^1$ sequence sandwiched between two $\pi/2$ pulses (bracketed scheme).

Experimental Section

NMR Setup. We used a Varian/Chemagnetics Infinity-plus spectrometer with a field of 9.4 T, using a CP/MAS probe with a 4 mm diameter rotor. Strips of P(3HB) films with a length of 10 mm were put into the sample rotors. The samples were rotated at a spinning speed of 14.988 kHz. Figure 4 shows an rf sequence for the 1D/2D NMR observations. The ^{13}C magnetization was prepared by ramped cross-polarization (RAMP-CP) with a contact time of 2 ms,[28] in which a ^{13}C rf field with a constant strength of 88 kHz was used and a ^{1}H rf field was varied from 117 to 100 kHz. The 1D NMR spectra were observed immediately after RAMP-CP. The 2D NMR spectra were observed adding a γ-encoding σ_2 recoupling sequence sandwiched by a pair of $\pi/2$ pulses to the 1D NMR sequence; the information on σ_2 ($\bar{\sigma}$) is encoded during the t_1 (t_2) dimension. Two-pulse phase-modulated (TPPM) decoupling[29] was applied throughout the t_1 and t_2 dimensions. A ^{1}H rf strength of 91 kHz was used in the t_2 dimension, and the strength was increased to 156 kHz in order to avoid ^{1}H−^{13}C recoupling in the t_1 dimension.[30] We observed the 2D $\sigma_2/\bar{\sigma}$ spectra by applying 2D Fourier transformation to the obtained free-induction-decay set. We used a recently developed modulated rf sequence to achieve γ-encoding σ_2 recoupling.[25] We used the $MR6_5^1$ sequence with the parameters of $g_{s1} = -0.33$, $g_{s2} = -2.6$, and $g_{s3} = -1.1$ (details are given in ref 25). While the cycle time of the $MR6_5^1$ sequence is $5\tau_r$, where $\tau_r = 2\pi/\omega_r$ is that of sample rotation, the t_1 time was increased in $5\tau_r/3$ steps. This sampling scheme triplicates the σ_2

bandwidth without significantly affecting the line shape.[25,31] Although $MR6_5^1$ decouples the $\bar{\sigma}$ and σ_1 terms in zeroth-order average Hamiltonians, higher order average Hamiltonians including the $\bar{\sigma}$ and σ_1 terms can affect the $\sigma_2/\bar{\sigma}$ spectra. To minimize this effect, we used a β_{RL} angle close to $\pi/2$, where the σ_1 term is minimized (see eq 3). Moreover, this maximizes the area of the $\sigma_2/\bar{\sigma}$ spectra; the angular resolution of (α_{PR}, β_{PR}) is maximized. The β_{RL} angle was determined by comparing the ^{13}C carbonyl spectra of glycine observed under OMAS and static conditions. β_{RL} was set to 90.0°. The effects of $\bar{\sigma}$ can almost be removed by adjusting the resonance offset within $\pm 0.2\omega_r$ from $\bar{\sigma}$.[25] We individually observed $\sigma_2/\bar{\sigma}$ spectra with irradiation at 130.0 and 180.0 ppm. We can obtain $\sigma_2/\bar{\sigma}$ signals with the resonance offset within $\pm 0.2\omega_r$ from $\bar{\sigma}$, by properly combining the spectra observed at 130.0 ppm and those at 180.0 ppm. Each 2D experiment took 14−18 h.

Sample Preparation. Ultrahigh-molecular-weight P(3HB) (UHMW-P(3HB)) samples were produced by *Escherichia coli* XL-1 Blue containing a stable plasmid pSYL105 bearing *Ralstonia eutropha* H16 (ATCC17699) PHB biosynthesis gene operon *phaCAB*, according to the method reported previously.[11] The weight-average-molecular-weight and polydispersity of UHMW-P(3HB) were determined to be 5.3×10^6 and 1.7, respectively. No ^{13}C labeling was applied.

The films of UHMW-P(3HB) were prepared by a conventional solvent-casting technique from a chloroform solution, using glass Petri dishes as casting surface. The melt-crystallized films were prepared by melting solvent-cast films in a hot press at 200 °C for 30 s and subsequently crystallizing them in an autoclave at 100 °C for 2 h. On the other hand, the amorphous preform films were prepared by melting solvent-cast films in a hot press at 200 °C for 30 s and subsequently quenching them with iced water. These amorphous preforms were oriented by cold drawing to 1000% of their initial length in iced water and were annealed in an autoclave at 100 °C for 2 h with weak tension to increase the crystallinity. In the case of two-step drawing, before annealing, a further 150% drawing was applied to 1000% cold-drawn films at room temperature. All samples were used after aging for at least 1 week at room temperature.

Wide-Angle X-ray Diffraction. X-ray fiber diagrams of P(3HB) samples were recorded in an evacuated flat-plate camera on a Fuji Imaging Plate BAS-SR 127, using Ni-filtered Cu Kα radiation with a Rigaku RINT UltraX 18 type X-ray generator operated at 40 kV and 110 mA.

Results and Discussion

X-ray diffraction diagrams for melt-crystallized, cold-drawn, and two-step-drawn films of UHMW-P(3HB) are shown in parts a, b, and c of Figure 5, respectively. Well-defined Debye−Scherrer rings are shown in Figure 5a, which indicates that the melt-crystallized film has a high crystallinity and random orientations of the α-form lamellar crystal. Figure 5b,c indicates that both of the stretched films were well oriented by cold-drawing and two-step-drawing. All of the reflections in the X-ray fiber diagram for the cold-drawn film presented in Figure 5b were indexed with the orthorhombic unit cell parameters of the α-form crystals: $a = 0.576$ nm, $b = 1.320$ nm, and c(fiber axis) $= 0.596$ nm, as reported previously.[16] However, the X-ray fiber diagram of the two-step-drawn film (Figure 5c) showed a new equatorial reflection derived from the planar zigzag conformation (*β*-form), together with the 2/1 helix conformation (α-form). These three kinds of films were used for the NMR experiments in this study.

We determined the CSA principal values of the carbonyl carbon in the UHMW-P(3HB) samples. We used the samples with ^{13}C in natural abundance. We observed the ^{13}C NMR spectrum under the static conditions for the melt-crystallized UHMW-P(3HB) films in which the crystals are uniformly

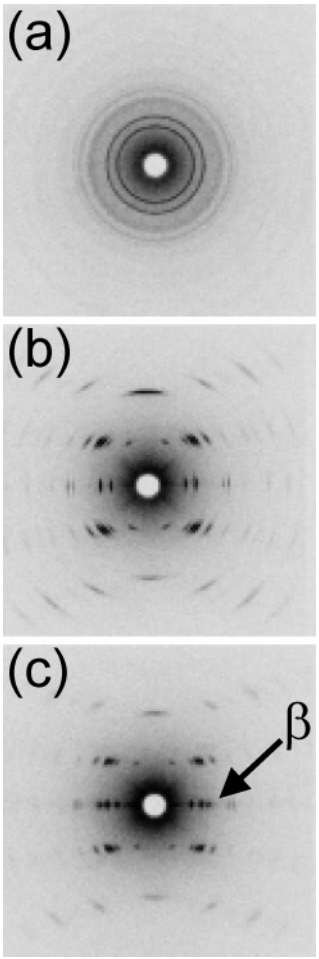

Figure 5. Wide-angle X-ray fiber diagrams of the melt-crystallized (a), cold-drawn (b), and two-step-drawn (c) UHMW-P(3HB) films. The drawn axis is vertical in (b) and (c). The arrow indicates a typical equatorial reflection of the planar zigzag conformation (*β*-form).

distributed (Figure 1). While the signals are broadened due to CSA, the signals of the carbonyl carbon appear separately from those of the aliphatic carbons in the spectrum. We determined the carbonyl ^{13}C CSA principal values of (σ_{11}, σ_{22}, σ_{33}) = (260.5, 139.0, 109.8) ppm for the α-form, by simulating the 1D powder pattern. The ^{13}C MAS NMR spectrum shows that the isotropic shift of a carbonyl carbon is the same for both the α-form and *β*-form in P(3HB). Since both the principal values and the isotropic shift for the carbonyl carbon are sensitive to the hydrogen-bonding structure of the C═O moiety,[32] we can convincingly assume that the CSA principal values of *β*-form are identical to those of α-form. We used the principal values of the melt-crystallized UHMH-P(3HB) films in the following calculations.

We confirmed that the $\sigma_2/\bar{\sigma}$ spectra are correctly obtained by the sequence given in Figure 4. First, we observed the 1D and 2D spectra (Figure 6a) of the melt-crystallized UHMW-P(3HB) films. Only the carbonyl region is shown. While the MAS NMR method provides sharp peaks, the 1D OMAS spectrum shows a broad 1D powder pattern due to CSA. This pattern is similar to that of the static sample, but its shape is scaled by sample rotation. The experimental 2D spectra yielded the characteristic powder patterns. The patterns show a parallelogram shape in the regions enclosed by the dashed lines, where the resonance offset is within $\pm 0.2\omega_r$ from $\bar{\sigma}$, although the powder patterns beyond the enclosed region deteriorate. This result confirms the theoretical pattern as pointed out in refs 23 and 25. We calculated the simulated 1D $\bar{\sigma}$ and 2D $\sigma_2/\bar{\sigma}$ spectrum (Figure

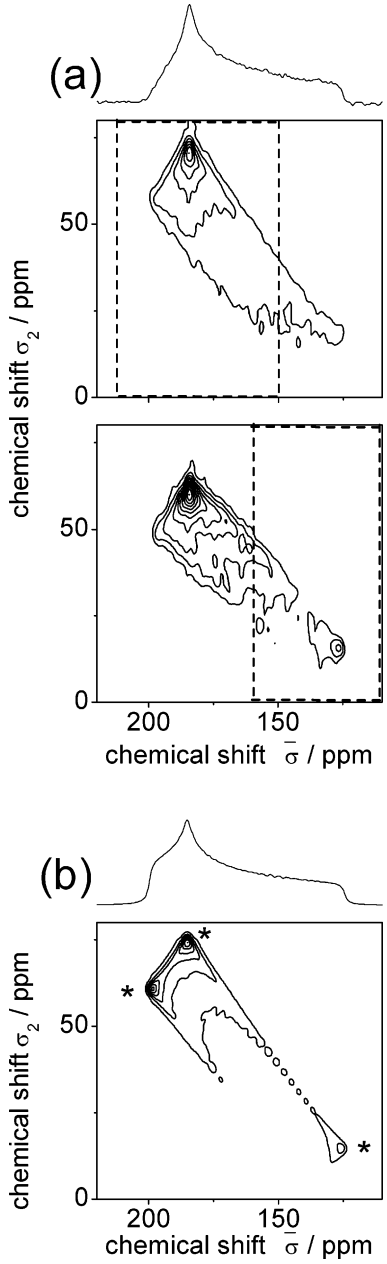

Figure 6. 1D and 2D ^{13}C OMAS NMR spectra of the melt-crystallized UHMW-P(3HB) films. Only the carbonyl region is shown. The experimental spectra (a) were observed at a spinning frequency of 14.988 kHz. A ^{13}C rf field was applied at 180.0 ppm (upper 2D) and 130.0 ppm (lower 2D), and the region where the rf-field was applied within $\pm 0.2\omega_r$ from $\bar{\sigma}$ is enclosed with dashed lines. The simulated spectra (b) were calculated under the assumption that the molecules are uniformly distributed.

6b) of the melt-crystallized UHMW-P(3HB) films. Assuming that the orientation of the crystals is uniformly distributed, we used the distribution of eq 8 in the calculations. The simulated 1D spectrum well agrees with the experimental spectrum. In the 2D spectrum, the ridges appear on the edge of the powder pattern, and three peaks appear at the three apices (asterisk in Figure 6b). These ridges and peaks are derived from the fact that the Jacobian determinant vanishes at those points;[23,25] the angular dependence of the resonance frequency is small near the angles corresponding to those singularities. Thus, the singularities appear even for uniformly distributed samples. The agreement between the simulated 2D spectrum and the experimental spectra in the enclosed region is also good; the effects of resonance offset and the σ_1 terms are well removed. Thus,

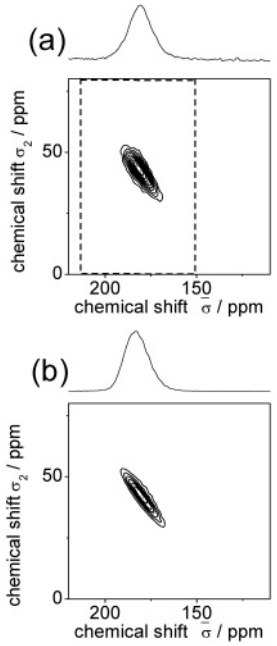

Figure 7. 1D and 2D ^{13}C OMAS NMR spectra of the cold-drawn UHMW-P(3HB) films. Only the carbonyl region is shown. The experimental spectra (a) were observed at a spinning frequency of 14.988 kHz. A ^{13}C rf field was applied at 180.0 ppm, and the region where the rf field was applied within $\pm 0.2\omega_r$ from $\bar{\sigma}$ is enclosed with dashed lines. The simulated spectra (b) were calculated using (α_{PC}, β_{PC}) = (14°, 32°), which gives the minimum RMSD value and the distribution function of eq 5 with $\sigma_{\beta_{CR}} = 0.10$.

we can correctly obtain 2D $\sigma_2/\bar{\sigma}$ spectra by selecting the proper regions of the spectra.

We observed the 1D ^{13}C NMR spectrum of the cold-drawn UHMW-P(3HB) film, which consists only of α-form (Figure 7a). The spectrum shows a sharp peak at 180 ppm, being completely different from that of the melt-crystallized sample. This indicates that the molecular chains uniaxially align along the drawn axis as mentioned in the NMR background section. The 2D NMR spectrum of the cold-drawn UHMW-P(3HB) film was observed to determine the molecular conformation (Figure 7a). The ^{13}C rf field was applied at 180.0 ppm. A peak appeared in the 2D spectrum, which can be a signal from α-form. The 2D peak is broadened due to the distribution of the *c*-axis in the rotor-fixed frame. The peak position is different from those of the three peaks observed for the melt-crystallized UHMW-P(3HB) films. The peak in Figure 7a is not derived from vanishing Jacobian but arises from the uniaxial molecular orientation around specific (α_{PR}, β_{PR}) angles. To obtain (α_{PC}, β_{PC}), we calculated the spectra for various (α_{PC}, β_{PC}) angles using the distribution function of eq 5 with $\sigma_{\beta_{CR}} = 0.10$. The full width at half-maximum of the distribution function is $\Delta\beta_{CR} = 2(2 \ln 2)^{1/2}\sigma_{\beta_{CR}} = 13°$.[26] The plot of the root-mean-squared deviation (RMSD) between the experimental spectra and the calculated spectra is given in Figure 8. Minimum RMSD structures were obtained for (α_{PC}, β_{PC}) = (14°, 32°). Note that the precision of the α_{PC} angle is rather low, since the spectral intensity spans the area where the ridges appear for the melt-crystallized UHMW-P(3HB) films, i.e., the area where the angular resolution is low. Both the 1D simulated spectrum for (α_{PC}, β_{PC}) = (14°, 32°) and the 2D one agree well with the experimental spectra (Figure 7b). Some molecular models of P(3HB) crystals were proposed on the basis of WAXD observations. Yokouchi and co-workers proposed a molecular model for α-form of P(3HB) from a WAXD observation of hot-drawn P(3HB) fibers. The model was constructed using the standard

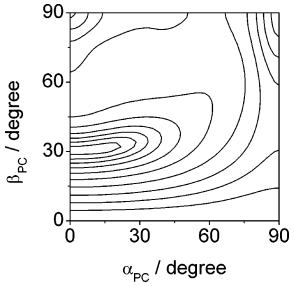

Figure 8. RMSD plot between the calculated and experimental 2D spectra of the cold-drawn UHMW-P(3HB) films.

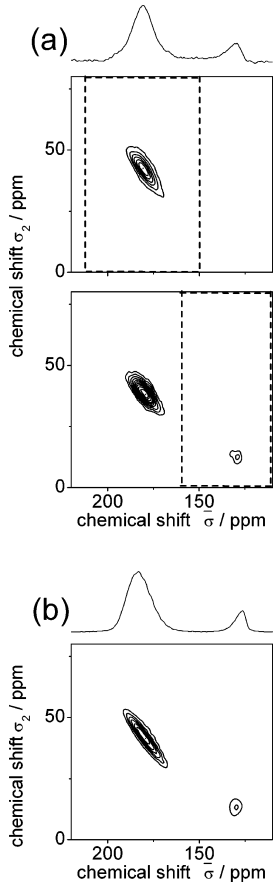

Figure 9. 1D and 2D ^{13}C OMAS NMR spectra of the two-step-drawn UHMW-P(3HB) films. Only the carbonyl region is shown. The experimental spectra (a) were observed at a spinning frequency of 14.988 kHz. A ^{13}C rf field was applied at 180.0 ppm (upper 2D) and 130.0 ppm (lower 2D), and the region where the rf field was applied within $\pm 0.2\omega_r$ from $\bar{\sigma}$ is enclosed with dashed lines. The simulated spectra (b) were obtained by adding the simulated spectra for α-form (Figure 7b) to the spectra calculated using (α_{PC}, β_{PC}) = (10°, 76° (104°)), which gives the minimum RMSD value and the distribution function of eq 5 with $\sigma_{\beta_{CR}} = 0.07$.

bond lengths, bond angles, and plausible internal rotation angles to satisfy the observed fiber period (0.596 nm) with calculation of the structure factors of the equatorial reflections and layer reflections and was refined by the diagonal least-squares method.[16] We calculated the orientation of the O═C−C moiety in the crystal fixed frame, using the above models, and we obtained (α_{PC}, β_{PC}) = (26°, 31°) (Figure 2). The present results agree with the molecular model of α-form based on WAXD. Therefore, we assigned the signal to α-form.

Figure 9 shows the spectra of the uniaxially two-step-drawn UHMW-P(3HB) films. The WAXD diagram shows the reflections due to α-form as well as an additional reflection due to the introduction of *β*-form (Figure 5c). Thus, the two-step-drawn

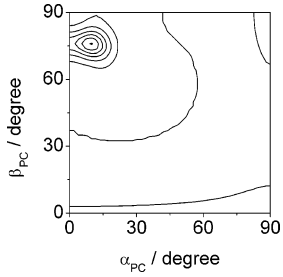

Figure 10. RMSD plot between the calculated and experimental 2D spectra of the two-step-drawn UHMW-P(3HB) films.

UHMW-P(3HB) film consists of both α-form and *β*-form. A new peak clearly appears at 130 ppm in the experimental 1D NMR spectrum in addition to the peak at 180 ppm, which is attributed to α-form (Figure 9a). We assigned the signal at 180 ppm to α-form by comparing the 2D spectrum of the cold drawn UHMW-P(3HB) films (Figure 7a) and that of the two-step-drawn UHMW-P(3HB) films obtained under irradiation of the rf field at 180.0 ppm (upper 2D in Figure 9a). Note that the peak at 130 ppm vanishes in the 2D spectrum due to the effect of resonance offset. To investigate the peak at 130 ppm, we observed the 2D spectrum by irradiating at 130.0 ppm (lower 2D in Figure 9a). The signal of α-form deteriorates due to the effect of resonance offset. The signal at $\bar{\sigma} = 130$ ppm gives a sharp peak in the 2D spectrum. The plot of the RMSD between the experimental and calculated spectra is given in Figure 10. In the calculation, the α-form signal is removed from the experimental spectrum. We used the distribution function of eq 5 with $\sigma_{\beta_{CR}} = 0.07$ ($\Delta\beta_{CR} = 9°$) for *β*-form. The minimum RMSD is obtained for (α_{PC}, β_{PC}) = (10°, 76° (104°)), which is completely different from that of α-form. Note that the β_{PC} angles of 76° and 104° give the same 2D spectra as mentioned before. Although the peak appears near the peak in Figure 6b, the overlap of the spectral intensity with the singularity is smaller than that for the cold-drawn UHMW-P(3HB). Thus, the (α_{PC}, β_{PC}) angle can be precisely determined. Figure 9b shows 1D and 2D simulated spectra of the two-step-drawn UHMW-P(3HB) film. We obtained these spectra by adding the signals due to α-form (Figure 7b) to the signals calculated using (α_{PC}, β_{PC}) = (10°, 76° (104°)). The simulated spectra agree well with the experimental results. We compared the present result with the *β*-form model proposed by Orts and co-workers. The model is based on the WAXD observation of cold-drawn PHB/V films consisting of both α-form and *β*-form. The model was obtained by a conformational analysis based on energy minimization of a single P(3HB) chain with the observed fiber repeat of PHB/V (0.460 nm) derived from the layer line streak.[17] Note that no other reflections were used to obtain the *β*-form model. We obtained (α_{PC}, β_{PC}) = (4°, 100°) for *β*-form from the molecular model (Figure 2). The agreement between the present result and the previously proposed model is satisfactory. While the WAXD results provide only the fiber repeat length, the present results reveal the orientation of the carbonyl carbon. This result strongly supports the molecular model of *β*-form. The differences between the present results and the WAXD based models both for α-form and *β*-form can be attributed to the difference in the detailed conformation and/or that in the PAS orientation in the molecular fixed frame for the carbonyl ^{13}C CSA interaction.

Conclusion

The 1D and 2D ^{13}C OMAS NMR spectra of the uniaxially drawn UHMW-P(3HB) samples with ^{13}C in natural abundance were observed. The signal of *β*-form in the two-step-drawn

UHMW-P(3HB) film was clearly distinguished from that of α-form by the 1D OMAS NMR method. The orientations of the carbonyl carbon both for α-form and *β*-form were determined by the 2D OMAS NMR method and compared to the WAXD-based models. Since the 2D OMAS NMR spectra was sensitive to the molecular conformation in uniaxially oriented samples, the 2D method can be useful to refine the molecular models proposed by the other methods such as WAXD. Note that the present approach does not require ^{13}C labeling. This approach can be applied not only to P(3HB) samples but also to any other uniaxially oriented samples.

References and Notes

(1) Lemoignei, M. *Bull. Soc. Chim. Biol.* **1926**, *8*, 770.
(2) Doi, Y. In *Microbial Polyesters*; VHC Publishers: New York, 1990.
(3) Lenz, R. W.; Marchessault, R. H. *Biomacromolecules* **2005**, *6*, 1.
(4) Holmes, P. A. In *Developments in Crystalline Polymers*; Bassett, D. C., Ed.; Elsevier Applied Science: New York, 1988; Vol. 2, pp 1−65.
(5) De Koning, G. J. M.; Lemstra, P. J. *Polymer* **1993**, *34*, 4089.
(6) Scandola, M.; Ceccorulli, G.; Pizzoli, M. *Macromol. Chem. Rapid Commun.* **1989**, *10*, 47.
(7) Gordeyev, S. A.; Nekrasov, Y. P. *J. Mater. Sci., Lett.* **1999**, *18*, 1691.
(8) Schmack, G.; Jehnichen, D.; Vogel, R.; Tandler, B. *J. Polym. Sci., Part B: Polym. Phys.* **2000**, *38*, 2841.
(9) Yamane, H.; Terao, K.; Hiki, S.; Kimura, Y. *Polymer* **2001**, *42*, 3241.
(10) Furuhashi, Y.; Imamura, Y.; Jikihara, Y.; Yamane, H. *Polymer* **2004**, *45*, 5703.
(11) Kusaka, S.; Iwata, T.; Doi, Y. *J. Macromol. Sci., Pure Appl. Chem.* **1998**, *A35*, 319.
(12) Aoyagi, Y.; Doi, Y.; Iwata, T. *Polym. Degrad. Stab.* **2003**, *79*, 209.
(13) Iwata, T.; Tsunoda, K.; Aoyagi, Y.; Kusaka, S.; Yonezawa, N.; Doi, Y. *Polym. Degrad. Stab.* **2003**, *79*, 217.
(14) Iwata, T.; Aoyagi, Y.; Fujita, M.; Yamane, H.; Doi, Y.; Suzuki, Y.; Takeuchi, A.; Uesugi, K. *Macromol. Rapid Commun.* **2004**, *25*, 1100.
(15) Tanaka, T.; Aoyagi, Y.; Doi, Y.; Iwata, T. *Sen'i Gakkaishi* **2004**, *60*, 309.
(16) Yokouchi, M.; Chatani, Y.; Tadokoro, H.; Teranishi, K.; Tani, H. *Polymer* **1973**, *14*, 267.
(17) Orts, W. J.; Marchessault, R. H.; Bluhm, T. L.; Hamer, G. K. *Macromolecules* **1990**, *23*, 5368.
(18) Iwata, T.; Fujita, M.; Aoyagi, Y.; Doi, Y.; Fujisawa, T. *Biomacromolecules* **2005**, *6*, 1803.
(19) Oas, T. G.; Hartzell, C. J.; McMahon, T. J.; Drobny, G. P.; Dahlquist, F. W. *J. Am. Chem. Soc.* **1987**, *109*, 5956.
(20) Hartzell, C. J.; Whitfield, M.; Oas, T. G.; Drobny, G. P. *J. Am. Chem. Soc.* **1987**, *109*, 5966.
(21) Takeda, N.; Kuroki, S.; Kurosu, H.; Ando, I. *Biopolymers* **1999**, *50*, 61.
(22) Asakura, T.; Yamazaki, Y.; Seng, K. W.; Demura, M. *J. Mol. Struct.* **1998**, *446*, 179.
(23) Nishiyama, Y.; Kubo, A.; Terao, T. *J. Chem. Phys.* **2003**, *119*, 3297.
(24) Deans, S. R. In *The Radon Transform and Some of Its Applications*; Wiley: New York, 1983.
(25) Nishiyama, Y.; Yamazaki, T.; Terao, T. *J. Chem. Phys.* **2006**, *124*, 064304.
(26) Schmidt-Rohr, K.; Spiess, H. W. In *Multidimensional Solid-State NMR and Polymers*; Academic Press: London, 1994.
(27) Bak, M.; Nielsen, N. C. *J. Magn. Reson.* **1997**, *125*, 132.
(28) Metz, G.; Wu, X.; Smith, S. O. *J. Magn. Reson. A* **1994**, *110*, 219.
(29) Bennett, A. E.; Rienstra, C. M.; Auger, M.; Lakshmi, K. V.; Griffin, R. G. *J. Chem. Phys.* **1995**, *103*, 6951.
(30) Ishii, Y.; Ashida, J.; Terao, T. *Chem. Phys. Lett.* **1995**, *246*, 439.
(31) Levitt, M. H. In *Encyclopedia of Nuclear Magnetic Resonance*; Grant, D. M., Harris, R. K., Ed.; Wiley: Chichester, 2002; Vol. 9, pp 165−196.
(32) Asakawa, N.; Kameda, T.; Kuroki, S.; Kurosu, H.; Ando, S.; Ando, I.; Shoji, A. *Annu. Rep. NMR Spectrosc.* **1998**, *35*, 55.

MA060291H